The near ultraviolet spectrum of the FCO radical: Re-assignment of transitions and predissociation of the electronically excited state

Wendy H. Howie, Ian C. Lane, and Andrew J. Orr-Ewing

Citation: The Journal of Chemical Physics **113**, 7237 (2000); doi: 10.1063/1.1313541
View online: http://dx.doi.org/10.1063/1.1313541
View Table of Contents: http://scitation.aip.org/content/aip/journal/jcp/113/17?ver=pdfcov
Published by the AIP Publishing

The near ultraviolet spectrum of the FCO radical: Re-assignment of transitions and predissociation of the electronically excited state

Wendy H. Howie, Ian C. Lane, and Andrew J. Orr-Ewing[a)]
School of Chemistry, University of Bristol, Cantock's Close, Bristol BS8 1TS, United Kingdom

(Received 19 June 2000; accepted 8 August 2000)

Cavity ring-down spectra of the FCO radical, recorded over the wave number range 29 500–31 600 cm^{-1} reveal rotational structure of the electronically excited state for the first time. The spectra demonstrate the need for a complete re-assignment of the vibronic features: The rotationally resolved bands are successfully simulated as arising from *c*-type transitions from the ground $\tilde{X}\,^2A'$ state to the linear $^2A''$ component of the $\tilde{A}\,^2\Pi$ state. The bands are attributed to two overlapping vibrational progressions: one progression involves excitation of the F–C–O bending mode (v_3'), the other consists of a combination of v_3' and one quantum of the C–F stretch (v_2'). Sharp rotational structure is only observed for sub-bands with $K'=0$; bands with $K'>0$ are diffuse, indicating rapid, rotation induced predissociation. Band origins, rotational constants for the excited state, and spectral linewidths have been derived from the $K'=0-K''=1$ sub-bands. All rotational lines are somewhat broadened and there is evidence of linewidths that increase with N', and hence an additional rotation-induced predissociation mechanism. Vibrational frequencies and rotational constants are in excellent agreement with the predictions of *ab initio* calculations by Krossner *et al.*, J. Chem. Phys. **101**, 3973 (1994); **101**, 3981 (1994). The $\tilde{A}\,^2\Pi(A'')-\tilde{X}\,^2A'$ absorption shows characteristics of a transition between two Renner–Teller components and this interpretation is confirmed by careful examination of the electronic structure of the FCO ground state. Implications for assignments of absorption features at higher energy than the spectral region of the current study are discussed, and comparisons are drawn with the much studied electronic spectroscopy of both the HCO radical and the isoelectronic NO_2. © *2000 American Institute of Physics.* [S0021-9606(00)01541-5]

I. INTRODUCTION

The atmospheric breakdown of certain chlorofluorocarbons (CFCs) and CFC substitutes produces F_2CO or HFCO molecules which can undergo further photochemical or chemical decomposition to generate the fluoroformyl (FCO) radical.[1–3] FCO may thus play a role in the chemistry of Earth's atmosphere. Theoretical studies by Francisco *et al.*[4] suggest that the stratospheric lifetime of this radical is sufficiently long to allow bimolecular processes such as adduct formation with O_2, and this prediction prompted several experimental investigations of the kinetics of various reactions of FCO.[5–10] FCO radical chemistry may also be significant in other reactive environments: for example, it is thought to inhibit combustion in halogen-containing flames by removal of H atoms.[11,12]

Despite a need for an improved understanding of FCO chemistry in both atmospheric and combustion chemistry, high sensitivity spectroscopic probes of this radical have not, to date, been forthcoming. Attempts to measure laser induced fluorescence (LIF) spectra have proved unsuccessful,[13,14] and detection via electronic transitions has been limited to low-resolution absorption studies using ultraviolet (UV) lamps. Milligan *et al.*[15] first reported an absorption spectrum of FCO in a matrix-isolation study; the spectrum exhibited an extensive series of absorption features between 220 and 340 nm. A prominent progression of bands with intervals of ~650 cm^{-1} was attributed to excitation of the upper state-bending mode of FCO. An absorption spectrum of gas-phase FCO was obtained via flash photolysis of a mixture of N_2F_4, CO, and N_2,[16] and spanned twenty four bands over the wavelength range 220–340 nm which were divided into two progressions with intervals of ~650 cm^{-1}. The bands were not assigned, but, following an extension of the previous matrix-isolation studies, Jacox[17] proposed a division of the bands into three overlapping progressions. From reference to theoretical studies of the electronically excited states of FCO,[18] progressions I and II were assigned to combinations of the v_1 (C–O stretch) and the v_3 (FCO bend) modes of the $\tilde{B}\,^2A'$ state (using vibrational notation such that, for the ground electronic state, $v_1>v_2>v_3$). Progression III was assigned to absorption to the $\tilde{C}\,^2A''$ state. Chemiluminescence from electronically excited FCO was subsequently attributed to emission from the $\tilde{B}\,^2A'$ state[19] by reference to the matrix isolation studies. The assignments of Jacox were also adopted for gas-phase UV absorption spectra of FCO derived from the flash photolysis of F_2 or F_2CO in the presence of CO.[20] Figure 1, which is adapted from Ref. 20, shows part of the UV spectrum of gaseous FCO between

a)Author to whom correspondence should be addressed. Telephone: +44 117 928 7672; Fax: +44 117 925 0612. Electronic mail: a.orr-ewing@bris.ac.uk

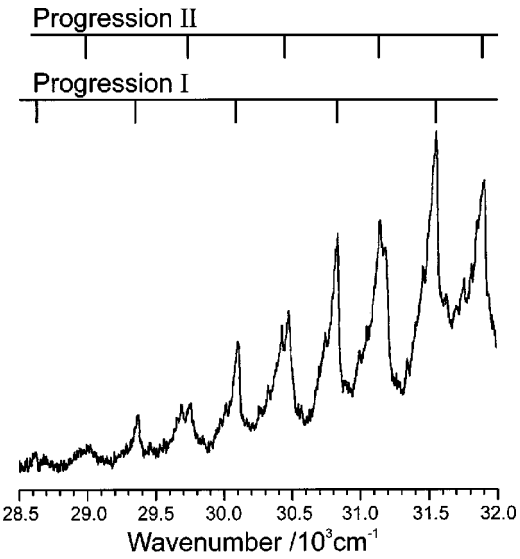

FIG. 1. The UV absorption spectrum of the FCO radical over the energy range 28 500–32 000 cm^{-1}. The spectrum is adapted from Ref. 20. The peaks evident in the spectrum have been labeled as members of progressions I and II, and were previously assigned to the $\tilde{B}\,^2A'-\tilde{X}\,^2A'$ transition (Refs. 17 and 20).

the wavelengths of 312 and 350 nm; the spectral features correspond to progressions I and II. In addition to the vibronic bands observed in the matrix-isolation studies,[15,17] a fourth progression at higher energy was identified and was interpreted as corresponding to excitation to a higher lying $^2A'$ electronic state.

Considerable efforts have been made to record an LIF spectrum of FCO, but so far without success. Photolysis of CF_2HCl in the presence of O atoms resulted only in LIF spectra of hot bands of CF_2.[13] Recently reported LIF features,[14] assigned to FCO but differing in appearance from the UV absorption spectra in the same wavelength region, have since been shown to originate from the CH_2CFO radical,[21–24] which was formed as a contaminant in the preparation process. The failure to observe FCO via LIF is most probably because of rapid predissociation of the electronically excited states.

The structure of the ground electronic state, and the frequencies of all three vibrational modes have been derived from infra-red diode laser studies.[25] As a consequence of the difficulties in producing a clean source of FCO combined with the limited resolution available to previous experiments, however, no rotational structure within the electronic spectra has so far been reported or analyzed. In this paper, we present a rotational analysis of six vibronic bands of FCO at wavelengths from 316–338 nm, observed at high resolution using cavity ring-down spectroscopy (CRDS).[26,27] Analysis of spectra gives rotational constants and a definitive and completely revised assignment for the upper state, as well as lifetimes and much refined values of band origins for the different vibrational states.

To facilitate the assignment of experimental data, there are several theoretical determinations of the energetics of the low lying electronically excited states of FCO. The first interpretation[17] of the FCO spectrum (as discussed above) was guided by calculations performed at the CNDO/CI level of approximation, together with suggested assignments of the UV absorption features to $2\,^2A''-\tilde{X}\,^2A'$ and the $2\,^2A'-\tilde{X}\,^2A'$ transitions.[18] Later calculations, performed using Møller–Plesset perturbation theory,[28] found the ground ($\tilde{X}\,^2A'$) state of FCO to derive from one component of a $^2\Pi$ state in linear geometry, just as is observed for HCO.[29] Krossner *et al.*[30,31] undertook multireference single and double-excitation configuration interaction (MRD-CI) calculations and predicted the form of the absorption spectrum, but maintained the earlier spectroscopic assignments of transitions. In contradiction to the previous studies, the MRD-CI calculations predicted that the ground electronic state, which correlates adiabatically to $CO(X\,^1\Sigma^+)+F(^2P)$ fragments as the F–C bond is extended, is derived from a $^2\Sigma^+$ state in linear geometry. The spectral assignments were questioned by a more recent computational study[32] which, on purely energetic grounds, argued that progressions I and II be attributed to excitation to the linear $^2A''$ component of the $\tilde{A}\,^2\Pi$ state. The predictions of vibrational frequencies from this study were, however, in poor agreement with experimental data. We have further explored the *ab initio* calculation of the low lying electronic states at various levels of theory to clarify the nature of the electronic structure of the ground state and to assist with interpretation of the spectroscopic data presented here and in previous studies.

II. EXPERIMENT

Experiments were conducted in a cavity-ring down apparatus with the facility for photolytic production of free radicals. Many of the features of the experiment have been described previously[33,34] and only the details specific to the formation and detection of FCO are presented here.

FCO radicals were probed by the frequency doubled (in KDP) output of a dye laser (Spectra Physics PDL-3) operating with DCM, or a cocktail of LDS 698 and DCM dyes to give additional spectral coverage. The dye laser was pumped by the 532 nm output of a Nd:YAG laser (Quantel YG680). Typical UV pulse energies were 1 to 2 mJ, and the UV radiation was introduced into the ring-down cell through one of a pair of carefully aligned, high-reflectivity (HR) mirrors (Research Electro Optics): the mirrors employed in this work had reflectivity $R\sim0.9993$ at 325 nm. The ring-down cell was constructed from a 1.5 m long glass vacuum cell, and the two HR mirrors acted as vacuum windows. The $1/e$ ring-down time for the empty cavity was $\sim7\ \mu s$, corresponding to a pathlength of 2.1 km. A photomultipier tube (PMT) monitored the exponential decay with time of the UV intensity transmitted through the exit mirror of the ring-down cell; this decay resulted from a combination of mirror losses and FCO absorption. The decaying signal was digitised on an oscilloscope (LeCroy 9400) and transferred to a PC for analysis. The exponential decay rate coefficient gives a quantitative measure of the absorption coefficient of the gas in the cell and was plotted against wavelength to obtain a spectrum. An accurate calibration of the scanning wavelength, which ranged from 316–338 nm, was obtained by using part of the

dye laser fundamental output to record simultaneously both an I_2 LIF spectrum and the transmission fringes of an etalon (free spectral range 0.492 cm^{-1}).

FCO was generated from the photolysis of oxalyl fluoride, $C_2F_2O_2$, (PCR, 97%) diluted to 50% in argon, using 266-nm radiation from a frequency quadrupled Nd:YAG laser (Quanta Ray DCR 11): Typical energies were 5–10 mJ in a ''donut'' shaped circular beam, 1 cm in diameter. The photolysis laser entered the ring-down cell slightly off axis and intersected the path of the probe beam for much of the length of the spectrometer. A continuous flow of $C_2F_2O_2-Ar$ gas mixture was regulated by a needle valve and was evacuated from the cavity 1 m downstream from the input port. A further flow of nitrogen gas was introduced in front of both HR mirrors to prevent accumulation of deposits, and to promote the thermalisation of the photolytically generated FCO. The optimum signal to noise ratio was achieved with flows of the $C_2F_2O_2-Ar$ gas mixture and N_2 in a ratio of 1:10, and the exhaust rotary pump throttled to give a total system pressure of 50 Torr. The maximum FCO signal was detected when the delay between the photolysis laser and the probe laser was ~4 μs. Parent ($C_2F_2O_2$) absorption was identified from baseline scans for which 266 nm photolysis radiation was not introduced into the apparatus.

III. RESULTS

CRDS has been used to record spectra at high-resolution of six FCO absorption bands in the wavelength range of 316–338 nm. The frequencies of the bands agree with those observed in part of the low resolution UV gas-phase absorption spectrum recorded by Maricq *et al.*[20] and shown in Fig. 1. The spectral range of the current work was limited for a combination of reasons: at wavelengths less than 316 nm the parent ($C_2F_2O_2$) absorption dominated the FCO spectra, and at wavelengths exceeding 338 nm the FCO signal became very weak.

Sample CRD spectra recorded over the wave number range 30 520–31 580 cm^{-1} are shown in Figs. 2–4. They exhibit rather different forms: Figures 2 and 4 are examples of sharp, strongly structured bands, whereas figure 3 illustrates a band with only weak structure superimposed on a double-humped diffuse background. An alternation between these two band types was observed for the six spectral features studied in detail: The bands with origins at ~31 560, 30 835, and 30 105 cm^{-1} are sharply structured; those at 31 195, 30 475, and 29 680 cm^{-1} are of the weakly structured type. Underlying all spectra and extending beyond the rotationally resolved regions are diffuse features that we assign to K sub-band structure.

Spectral analysis of the fine structure evident in both types of absorption bands was carried out using an asymmetric top spectral simulation program. This program employs the rotational Hamiltonian

$$\hat{H}=A\hat{N}_a^2+B\hat{N}_b^2+C\hat{N}_c^2+\hat{H}_{\text{cent}}, \tag{1}$$

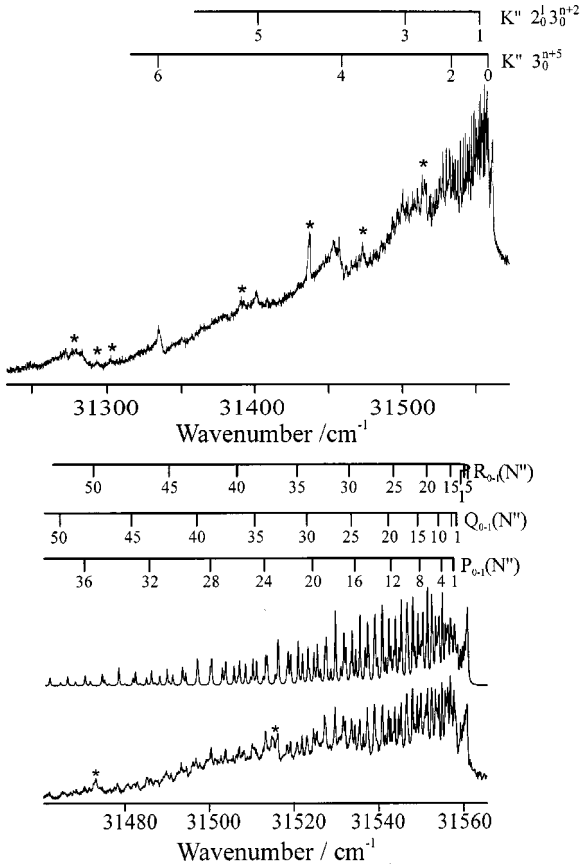

FIG. 2. Top: CRD absorption spectrum of the FCO $\tilde{A}\,^2\Pi(A'')-\tilde{X}\,^2A'$ transition in the wave-number range 31 228–31 578 cm^{-1}. The spectrum shows a sharp, strongly structured band with origin at 31 558.44(5) cm^{-1}. This band sits on top of diffuse features which are attributed to excitation to levels with $K'>0$; odd and even values of K' arise from two different overlapping vibrational progressions (see text) and the approximate sub-band positions are labeled according to their likely K'' values [estimated using Eq. (4)] and vibrational band (with n an even number). Bottom: the rotationally resolved region of the spectrum is shown on an expanded scale together with a spectral simulation (above) using the constants summarized in Table I. The combs above the spectrum indicate the assignments of the rotational features. The simulation is of a $K'=0-K''=1$ transition with c-type transition moment and a temperature of 300 K. A perturbation causes a shift of lines which terminate at $N'=14$ by ~0.3 cm^{-1}. Simulation line shapes include a Gaussian component of FWHM 0.08 cm^{-1} (laser linewidth) and a Lorentzian component of FWHM 0.25 cm^{-1}. Features marked with an * are due to absorption by $C_2F_2O_2$, the FCO precursor.

where A, B, C are the rotational constants about the three principal axes of the molecule, and the centrifugal distortion operator is given by

$$\hat{H}_{\text{cent}}=-\Delta_N\hat{N}^4-\Delta_{NK}\hat{N}_a^2\hat{N}^2-\Delta_K\hat{N}_a^4-2\delta_N\hat{N}^2(\hat{N}_b^2-\hat{N}_c^2)$$
$$-\delta_K[(\hat{N}_b^2-\hat{N}_c^2)\hat{N}_a^2+\hat{N}_a^2(\hat{N}_b^2-\hat{N}_c^2)]. \tag{2}$$

Ground electronic state rotational constants were taken from the infrared diode-laser absorption study by Nagai *et al.*[25] A first approximation of the electronically excited state rotational constants A', B', C' and the origin for the $K'-K''$ sub-band, $T_{K'-K''}$, was obtained using by-eye comparison of the simulated and experimental spectra. Simulations and the subsequent fitting described below neglected the effect of the unpaired electron spin in both the ground and excited states. The simulations revealed that the FCO bands are carried by a

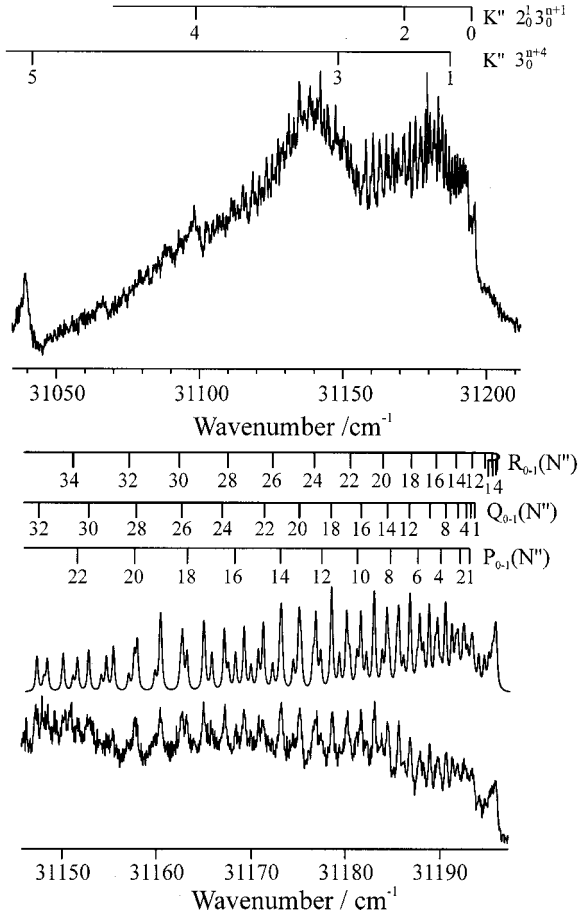

FIG. 3. Top: CRD spectrum of the FCO $\tilde{A}\,^2\Pi(A'')-\tilde{X}\,^2A'$ transition in the wave number region 31 036–31 213 cm^{-1}. The double-humped diffuse structure underlies a weak, sharply structured band with origin at 31 193.80(4) cm^{-1}. Bottom: expanded view of the rotationally structured region together with a simulated spectrum (above). The simulation was performed as described in the text and the caption to Fig. 1. Combs above the spectrum indicate the rotational line assignments. The simulation contains Gaussian (FWHM 0.08 cm^{-1}) and Lorentzian (FWHM 0.30 cm^{-1}) contributions to the line shapes. Diffuse features are labeled with numbers indicating the likely K'' values and vibrational band assignments, as explained in the caption to Fig. 1.

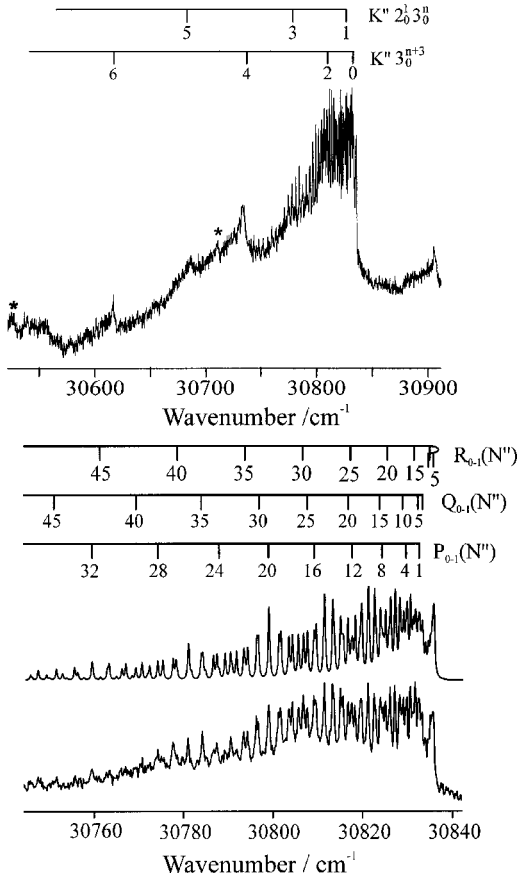

FIG. 4. Top: CRD spectrum of the FCO $\tilde{A}\,^2\Pi(A'')-\tilde{X}\,^2A'$ transition in the wave number region 30 520–30 912 cm^{-1}. Bottom: Expanded view of the structured region with origin at 30 833.49(5) cm^{-1} and spectral simulation (above). The simulation contains Gaussian (FWHM 0.08 cm^{-1}) and Lorentzian (FWHM 0.35 cm^{-1}) contributions to the line shapes. Other details are as for Figs. 2 and 3.

c-type transition moment and that excitation must be to a linear upper state: faithful reproduction of most spectral features was achieved in this way and permitted a first assignment of rotational lines. Further refinements to the simulated spectra were achieved by the assignment of spectral lines and the floating of excited state constants (B', $\Delta_{N'}$ and $T_{K'-K''}$) in a least squares fitting program to optimize computed line positions. The value of A' was fixed at a very large number ($>$500 cm^{-1}) and B' and C' were constrained to be equal, as required for a linear upper state. Provided A' was chosen to be sufficiently large, its precise value did not effect the derived values of the other constants. Figure 5 shows an expanded view of the band with origin at 30 104.20(3) cm^{-1} to illustrate the quality of the fits. The simulated spectra neglect spin-rotation coupling, but the excellent agreement between the simulations and experimental spectra in Figs. 2–5 demonstrate the negligible effect of the unpaired electron spin on observed spectra. All the resolved lines can be assigned to $K_a'=0\leftarrow K_a''=1$ transitions of FCO. Therefore, the only distortion constant required in the fitting scheme was $\Delta_{N'}$: The upper state rotational levels within a sub-band were thus fitted to the expression

$$E(N',K')=B'N'(N'+1)-\Delta_N'N'^2(N'+1)^2. \qquad (3)$$

Rotational constants and band origins derived from the fits are reported in Table I, together with the errors in their values obtained from the fitting procedure.

Spectral simulations of the $(K'=0)$ FCO band with origin at $T_{0-1}=31\,558.44(5)$ cm^{-1} revealed a perturbation in absorption lines terminating at $N'=14$. We observed a shift in the $P(15)$, $Q(14)$, and $R(13)$ lines of $\sim$0.3 cm^{-1} to lower frequency than the predictions of the simulations, with nearby lines involving transitions to $N'=15$ and 13 perhaps showing small perturbations which cannot be quantified reliably. The perturbation is localized and causes line shifts rather than broadening, so the perturbing state must be sharp. There are several candidate states that may cause this localized perturbation of the $N'=14$ level: these include C–O stretch resonance levels of the ground electronic state persisting above the C–F bond dissociation limit, ''dark'' (i.e.,

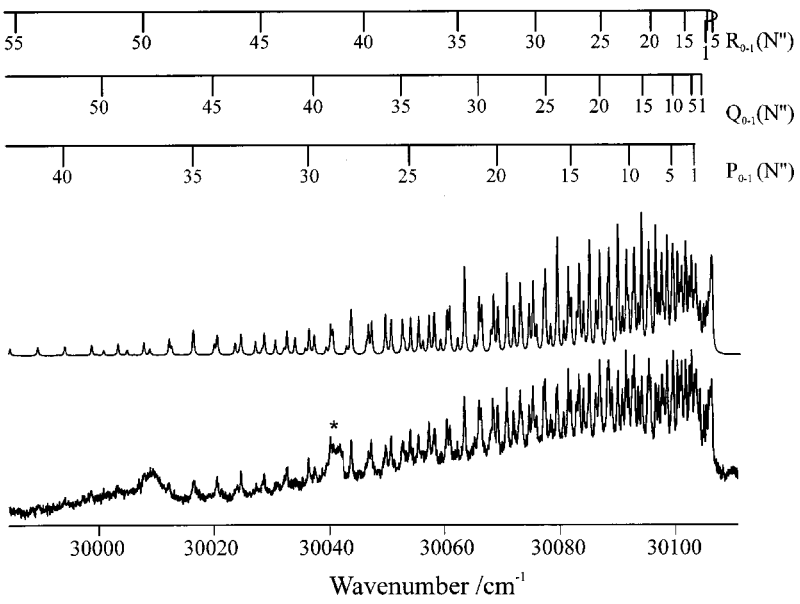

FIG. 5. CRD spectrum and simulation of the FCO $\tilde{A}\,^2\Pi(A'')-\tilde{X}\,^2A'$ transition in the vicinity of the $K'=0-K''=1$ sub-band with origin at 30 104.20(3) cm^{-1}. The simulation contains Gaussian (FWHM 0.08 cm^{-1}) and Lorentzian (FWHM 0.25 cm^{-1}) contributions to the line shapes. Other details are as for Figs. 2 and 3.

non-Franck–Condon active) vibrational levels of the $\tilde{A}$ state, or interaction with levels of a $^2A'$ state via out-of-plane rotation.

The K sub-bands underlying the structured FCO bands (Figs. 2–4) show no resolved structure apart from overlapping diffuse features and hence cannot be analyzed to obtain rotational constants. An estimate of the frequencies of the origins of the K sub-bands could, however, the made. The approximate locations of K sub-band origins were modelled (with neglect of rotational fine structure and spin–rotation effects) relative to an electronic and vibrational origin T_{ev} by

$$T_{K'-K''}=T_{ev}+sK'^2-(A''-\overline{B''})K''^2, \tag{4}$$

where $K_a\cong K''$ for a near-prolate asymmetric top and $K'=|\ell\pm\Lambda|$ is the sum of the component of vibrational angular momentum (ℓ) derived from the bending mode (v_3'), and the axial projection of the electronic orbital angular momentum (Λ): The latter takes the value $\Lambda=1$ for an upper state of Π symmetry. K' assumes odd or even values depending on the value of v_3': for an odd number of quanta of bend, ℓ is odd and K' is even, while for an even number of quanta of bend, ℓ is even and K' is odd. Figures 2–4 show examples of the K sub-bands with the proposed K'' transition assignments. The assignments suppose that s is much smaller than $A''-\overline{B''}$, as expected from estimates of this parameter made using formulas derived by Pople and Longuet-Higgins[35] based on an approximation of the bending potentials of the lower and upper Renner–Teller components as quartic functions. In the limit of the vibrational quantum number greatly exceeding the value of K, a straightforward prediction for the energy level pattern in the upper component is obtained which depends upon K'^2 and the parameters defining the bending potential function. Estimates of these parameters, and hence s were made using the methodology of Ref. 35, with barrier heights and equilibrium geometries derived from the *ab initio* calculations described in Sec. IV.

TABLE I. Origins (T_{0-1}) of the $K'=0-K''=1$ sub-bands (referenced to the energy of the $K''=1$ sub-level), and spectroscopic constants for the $K'=0$ levels of the $\tilde{A}\,^2\Pi(A'')$ state of FCO derived from fits to experimental spectra as described in the text. In the fits, B' and C' were constrained to be equal, and all parameters were insensitive to the precise choice of A', provided it was chosen to be greater than 500 cm^{-1}. The $\tilde{X}\,^2A'$ state constants used in the fits were (Ref. 25) $A''=6.377\,746$ cm^{-1}, $B''=0.382\,47$ cm^{-1}, $C''=0.360\,09$ cm^{-1}, $\Delta_{K''}=0.001\,318$ cm^{-1}, $\Delta_{N''}=410\times10^{-9}$ cm^{-1}, $\delta_{N''}=67.38\times10^{-9}$ cm^{-1}, $\delta_{K''}=2.669\times10^{-6}$ cm^{-1}. Errors for T_{0-1}, B' and $\Delta_{N'}$ were derived from the least-squares fits to experimental line positions. The ranges in Lorentzian components of linewidths (FWHM, Γ) were estimated by comparing simulated and experimental spectra, and do not allow for increased line broadening at high N'.

T_{0-1}/cm^{-1}	Band type	$B'=C'$/cm^{-1}	$\Delta_{N'}$/cm^{-1}	Γ/cm^{-1}
31 558.44(5)	Strong structure	0.3269(1)	[0][a]	0.25–0.30
31 193.80(4)	Weak structure	0.320 74(5)	[0][a]	0.25–0.30
30 833.49(5)	Strong structure	0.325 45(3)	$1.9(7)\times10^{-7}$	0.30–0.40
30 472.07(7)	Weak structure	0.319 66(1)	$2.3(2)\times10^{-6}$	0.40–0.55
30 104.20(3)	Strong structure	0.324 18(6)	$4.1(9)\times10^{-7}$	0.25–0.30
29 679.88(6)	Weak structure	0.319 06(23)	$5.0(2)\times10^{-8}$	0.45–0.50

[a][0] Constrained to be zero.

As a consequence of predissociation of the excited state of FCO, the bands exhibit a range of spectral linewidths and varying degrees of resolved rotational structure. Experimental linewidths result from a combination of a Gaussian component (consisting of the laser lineshape and Doppler broadening) of full width at half maximum (FWHM) 0.08 cm^{-1}, and a Lorentzian component arising from lifetime broadening of the upper state. For all the FCO bands, the Lorentzian component (with FWHM Γ) exceeds the Gaussian contributions to the linewidth. Simulations of the bands included both functional forms of line shape components, and Γ was varied to give the closest correspondence to the experimental FCO line shapes and band contours. The values of Γ (in cm^{-1}) are related to the lifetimes (τ) of the excited state levels via

$$\Gamma=\frac{1}{2\pi c\tau}, \tag{5}$$

where c is the speed of light. The resultant linewidths of the

FCO bands with $K'=0$ and lifetimes of the excited state levels are reported in Table I: It was impossible to deconvolute the spectral linewidths of the sub-bands with $K'>0$ because the bands are so diffuse, but since no rotational fine structure is observed in these bands we can place a lower limit of linewidth, (and hence an upper limit to the excited-state lifetime) on these bands of $\Gamma \geqslant 2.0\,\mathrm{cm}^{-1}$ ($\tau \leqslant 2.7$ ps). Note that the linewidth analysis completely neglects the possible effects of splitting of rotational lines by spin–rotation interactions in the doublet FCO radical. The values of spin–rotation constants for the ground electronic state[25] demonstrate that splittings will be much smaller than the experimental resolution (e.g., $\gamma(N''+\frac{1}{2})=0.006\,\mathrm{cm}^{-1}$ for $K''=1$, $N''=20$), and the spin–rotational coupling in the excited states is, by inference, assumed also to be weak. The rotational lines are observed to increase in width as the rotational quantum number N' increases: for example, for the band with origin at 30 104.20(3) cm^{-1}, the linewidth at $N'=12$ is 0.25 cm^{-1}, whereas for $N'=25$ our best estimate of the linewidth is 0.45 cm^{-1}. This broadening could be a consequence of the spin–rotation splitting becoming more evident as N' increases, but is more likely to be a result of a rotation-induced predissociation mechanism (see Sec. V C).

IV. *AB INITIO* CALCULATIONS

Extensive *ab initio* computational studies of the FCO radical have revealed much about the nature of the ground and first few electronic states, including electronic energies and symmetries, and vibrational frequencies of all three modes for each state. Rather than adopting the, $\tilde{A}$, $\tilde{B}$, and $\tilde{C}$ labels used to identify states in the spectroscopic studies, many of the publications based on *ab initio* calculations number the roots of A' and A'' symmetry with increasing energy as $\tilde{X}\,^2A'$, $2\,^2A'$,… and $1\,^2A''$, $2\,^2A''$,... respectively. In this work, we retain the spectroscopic labeling, and employ the numeric labels only when necessary to emphasise the energy ordering of states for calculations performed at FCO geometries other than the equilibrium geometry of the ground state.

The previous calculations do not agree on the energetic ordering of the low lying $^2\Pi$ and $^2\Sigma^+$ states in the linear geometry. Complete active space self-consistent field (CASSCF) calculations with geometry optimization and spin-projected fourth-order Møller–Plesset perturbation theory[28] predicted a $^2\Pi$ ground state, whereas computations at the MRD-CI level[30–32] with a double zeta $(9s5p)/[4s2p]$ basis set[36] (augmented by additional functions in Refs. 30 and 31) determined the $^2\Sigma^+$ state to be the lower in energy. The most recent calculations[32] show conical intersections between the two states. In the linear geometry, for the C–F distance ($R_{\mathrm{C-F}}$) fixed at its equilibrium value of 1.34 Å, the $^2\Pi$ state becomes the ground state for $R_{\mathrm{C-O}}>1.26$ Å. Similarly, for $R_{\mathrm{C-O}}$ fixed at the equilibrium value of 1.17 Å, the $^2\Pi$ state lies below the $^2\Sigma^+$ state for $R_{\mathrm{C-F}}<1.33$ Å. To establish the reliability of the previous calculations, and to try to clarify differences between their outcomes, we have also performed electronic structure calculations on the low-lying electronic states of FCO at a high level of theory. The range of geometries of our calculations is not as extensive as previous theoretical studies, but instead concentrates on the Franck–Condon region, the energetics at near linear geometries, the shapes of the potentials along the bending and C–F stretching coordinates for fixed C–O distances and the energy minima of excited states.

Calculations were performed using a triple-zeta aug-cc-pVTZ basis set,[37] with the *f* basis functions removed to reduce the computational time by ~50%. No additional diffuse atomic orbitals were added, nor were Rydberg molecular orbitals included in the active spaces employed because the focus of this study is on the valence electronic states. For the purposes of comparison with previous *ab initio* studies, C–F stretching potential curves were computed at the equilibrium C–O bond length (1.17 Å) for the ground state and for a bond angle of 120°. CASSCF wave functions were calculated including all the valence electrons and valence orbitals (seventeen electrons in twelve orbitals). Since there are likely to be Renner–Teller state pairs present in the valence states, the state-averaged CASSCF (SA-CASSCF) method was employed to minimize the total energy of all the electronic states specified, regardless of symmetry. The calculations were carried out using MOLPRO 98.1[38] on a Beowulf computer network that has been described previously.[39] A calculation including two $^2A'$ states and one $^2A''$ state resulted in a barrier to dissociation along the C–F bond coordinate on the ground electronic state surface. For more extended C–O bond lengths, the energy of the F+CO dissociation limit rose rapidly, and the well behind the barrier deepened. In addition, wells appeared in the two excited states calculated. The minimum of the $\tilde{X}\,^2A'$ state at the SA-CASSCF level ($E_h=-212.308\,779\,13$ hartrees) was calculated using the experimentally determined geometric parameters $R_{\mathrm{C-O}}=1.1678$ Å, $R_{\mathrm{C-F}}=1.3340$ Å, $\Theta=127.3°$. The SA-CASSCF level calculations placed the first dissociation limit (for $R_{\mathrm{C-O}}$ and Θ fixed at the above values) below the minimum energy of the FCO ground state, with an activation barrier of ~5800 cm^{-1} preventing spontaneous fragmentation of the radical.

Internally contracted, multireference CI (MRCI) calculations[40] were performed to improve the energetics of the potentials derived from the SA-CASSCF method. The MRCI calculations required considerable computational effort and thus, instead of using the whole valence space, the lowest two valence orbitals were closed in the MRCI step in addition to the three core orbitals. The effect of closing the lowest two orbitals was tested against a full valence calculation at the equilibrium geometry, and the resulting energy separation between the lowest two A' states was altered by just 6 cm^{-1}. The smallest closed orbital space used was (5,0), where the numbers in brackets are the number of included $a_1\,(a')$ and $a_2\,(a'')$ orbitals, respectively. The resulting computational time for two states of the same symmetry was about four days per point, calling the entire 512 Mb RAM of a single Beowulf node. The closed orbital space was (6,0) for calculations including three states of the same symmetry. Figure 6 displays the results of the MRCI calculations and reveals that the barrier predicted at the SA-CASSCF level is removed by dynamic electron correlation. It is thus

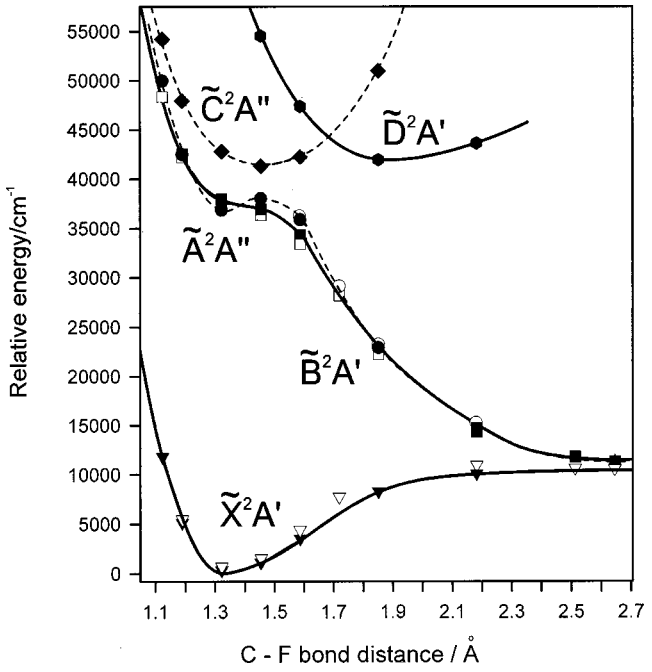

FIG. 6. MRCI calculations for the C–F stretching potentials of the lowest valence states calculated at a fixed bond angle of 120° and $R_{C-O}=1.1678$ Å. Open symbols: *ab initio* points from a SA-CASSCF calculation over two $^2A'+$one $^2A''$ state followed by the MRCI stage. Solid symbols: SA-CASSCF calculation over three $^2A'+$two $^2A''$ states followed by MRCI. Lines are sketched potential energy curves from the three $^2A'+$two $^2A''$ states calculation: solid curves represent $^2A'$ states and dashed curves are $^2A''$ states. Note that the $\tilde{A}\,^2\Pi(A'')$ state is slightly bound, but the $\tilde{B}\,^2A'$ state merely has a point of inflexion.

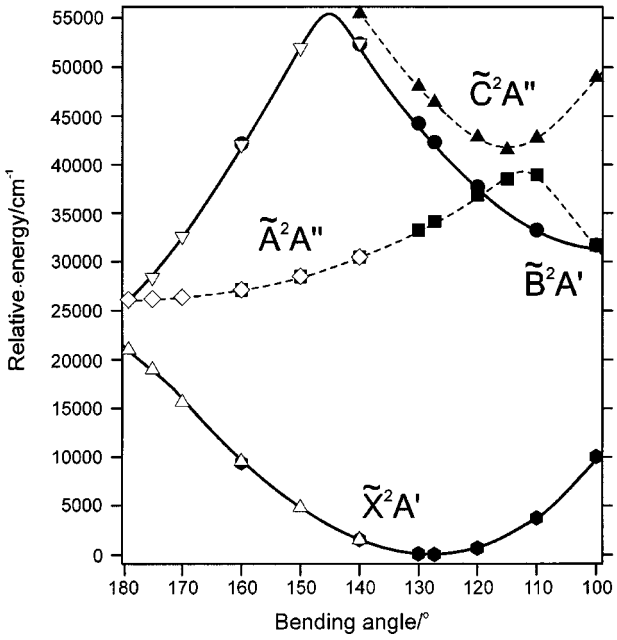

FIG. 7. MRCI calculations for the bending potentials of the FCO radical calculated with the C–F and C–O bond lengths fixed at the experimentally determined equilibrium bond lengths for the $\tilde{X}\,^2A'$ state. For $179.99°<\Theta<140°$, two $^2A'$ and one $^2A''$ states are included (open symbols), while for $\Theta<160°$, calculations were performed for two $^2A'$ and two $^2A''$ states (black symbols). Solid curves are $^2A'$ states: dashed curves are $^2A''$ states.

evident that MRCI calculations are required to describe accurately the characteristics of the FCO electronic states. Unless stated otherwise, all reported MRCI energies include the Davidson correction.[41] For two $^2A'$ states in the calculation, the computed MRCI energy at the $\tilde{X}\,^2A'$ state minimum geometry specified earlier is $-212.784\,834\,3$ hartrees. The closing of the $6a_1$ orbital does, however, make noticeable changes to the shape of the potential (compare the open and solid symbols in Fig. 6), and therefore, for an accurate description, it is best to limit the closed orbital space to (5,0) or smaller.

Calculations were extended to explore the nature of the bending potentials of the ground and excited states at the equilibrium bond lengths of the ground state. SA-CASSCF potentials showed nonphysical undulations that could not be removed by increasing the number of states calculated or the active orbital space. This effect has been seen in similar calculations on HCO.[42] The SA-CASSCF wavefunctions were used as input to an MRCI calculation of two A' and one A'' state. At $\Theta<160°$, the calculation was extended to two A' and two A'' states. Figure 7 shows the results of the computed bending potentials, which, although smoother than those derived at the SA-CASSCF level, have vertical transition energies reduced by less than 2000 cm^{-1}. The curves illustrated in Fig. 7 agree closely with cuts through the potential-energy surfaces (PESs) calculated by Krossner *et al.*[30]

Calculation of the energetics of the $\tilde{A}\,^2\Pi(A'')$ state presented particular difficulties because the minimum in the bending coordinate lies at linear geometry, and comparison must be made between energies calculated for bent and linear arrangements. The minimum energy of the $\tilde{A}\,^2\Pi(A'')$ state for linear F–C–O was calculated at the MRCI level in C_{2v} symmetry (as required in MOLPRO for linear geometry); this state is responsible for the first $^2A''$ state at bent (C_s symmetry) geometries with $\Theta>115°$. The use of C_{2v} symmetry reduced substantially the time necessary to perform the CI calculation to ~4 h per point. The C–O and C–F bond lengths corresponding to the minimum energy in linear geometry (1.205 and 1.2847 Å, respectively) were then used in a MRCI calculation performed at a bond angle of 179.99° to compare the effects of calculations in C_{2v} and C_s symmetry. The $\tilde{A}\,^2\Pi(A'')$ state potential is relatively flat at geometries close to linear, so slight deviations from linearity should result only in very modest errors in the energy minimum when compared to the strictly linear configuration, but calculations in the two different symmetries differed considerably in resultant energies. In order that energies computed at linear geometry can be properly compared with those for bent configurations, all calculations were subsequently performed in C_s symmetry, with linearity well approximated by $\Theta=179.99°$. We note in passing that the C–O bond length obtained for the $\tilde{A}\,^2\Pi(A'')$ state minimum is almost identical to that measured spectroscopically for CO ($a\,^3\Pi$).[43]

At an FCO bond angle of 179.99°, the $\tilde{A}\,^2\Pi(A'')$ state minimum was computed to lie 25 115 cm^{-1} above the minimum of the ground state. The consistency between this energy value and that computed by Krossner *et al.* (who denoted the state as $1\,^2\Pi$), as well as the close similarities of

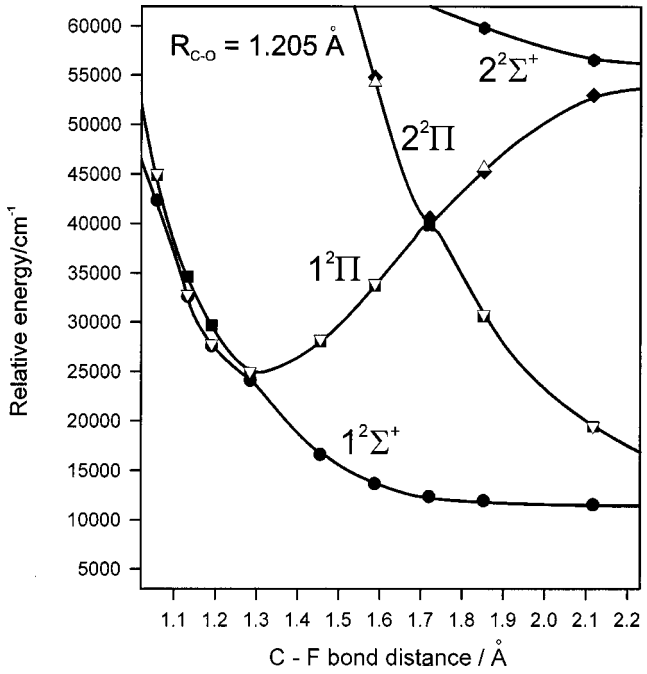

FIG. 8. C–F stretching potentials for the lowest six valence states (four $^2A'$ and two $^2A''$ states) at the near linear bond angle of 179.99°. Electronic states are labeled according to symmetry type in linear geometry and states of the same symmetry are numbered by energy ordering at $R_{C-F}=1.34$ Å. Points were calculated at the MRCI level with either six ($^2A'$) or five ($^2A''$) a' orbitals closed. Calculated $^2\Pi$ states (for true linear geometry) are revealed by a coincidence of $^2A'$ (solid symbols) and $^2A''$ (open symbols) energies. The adiabatic potential curves in C_s symmetry are sketched (solid lines) for the $^2A'$ states only.

calculated bending potentials, encouraged us to rely upon the predicted vibrational frequencies of Ref. 31 to avoid recalculation of a large number of *ab initio* points. The vibrational frequencies for the $\tilde{A}\,^2\Pi(A'')$ state presented in Ref. 32 differ from those of Krossner *et al.*, and do not match experimental observations.

Previous studies presented cuts through the C–F stretching potential at linear geometry for R_{C-O} fixed at the $\tilde{X}\,^2A'$ equilibrium value, but we have instead calculated such cuts with R_{C-O} corresponding to the minimum of the $\tilde{A}\,^2\Pi(A'')$ state (1.205 Å). Figure 8 shows the variations of the energies of the low-lying valence states with C–F bond length at an angle of 179.99°. The states are numbered by symmetry type according to their energy ordering at $R_{C-F}=1.34$ Å (the $1\,^2\Pi$ state is equivalent to the $\tilde{A}\,^2\Pi$ state). The $1\,^2\Sigma^+$ state, which evolves adiabatically into the $\tilde{X}\,^2A'$ state as the radical bends, is found to be purely repulsive along the R_{C-F} coordinate. There is an evident degeneracy of a pair of $^2A'$ and $^2A''$ components, indicative of a $^2\Pi$ state, and the lowest $^2\Sigma^+(A')$ state lies beneath this $^2\Pi$ state at most R_{C-F} values. This energy ordering at the geometry of the $\tilde{A}\,^2\Pi(A'')$ state minimum only arises, however, following inclusion of the Davidson or Pople corrections to the MRCI energies: a purely single and double excitation calculation predicts the reverse energy ordering. The calculations also demonstrate that these potentials cross at $R_{C-F}\sim 1.28$ Å. Though broadly in agreement with the results of Nanbu *et al.*[32] our calculations do not show any evidence for a well in the $1\,^2\Sigma^+(A')$ potential curve at our choice of R_{C-O}.

An estimate of the C–F bond dissociation energy was derived using the internally contracted MRCI method with the aug-cc-pVTZ basis set (*s*, *p*, *d* orbitals only) by determining the energy of the repulsive $\tilde{B}\,^2A'$ state potential (which is likely to be greater than the dissociation limit) and the $\tilde{X}\,^2A'$ state at large C–F bond lengths. Reliable energy values could not be obtained, however, beyond $R_{C-F}=2.646$ Å. The calculation determined the bond dissociation energy to lie within the range $10\,473\text{cm}^{-1}$ ($29.9\,\text{kcal mol}^{-1}$)$<D_e(\tilde{X}\,^2A')$ $<11\,269\,\text{cm}^{-1}$ ($32.2\,\text{kcal mol}^{-1}$). This value is in good agreement with the results of dissociative electron capture experiments,[44] ion–molecule collision studies[45] ($D_0=34\pm4\,\text{kcal mol}^{-1}$), and the lower limit of $28.9\pm2.9\,\text{kcal mol}^{-1}$ from a photoionization efficiency spectrum.[46] The results of our calculations are, however, smaller than a recent CCSD(T) calculation[47] ($D_0=35.4\,\text{kcal mol}^{-1}$) which included a spin–orbit correction and were extrapolated to the complete basis set limit (resulting in a deeper ground-state potential well).

The calculations performed in this work and in previous studies are vital for interpretation of the spectra presented in Sec. III. In the following section, the new spectroscopic data are discussed with reference to the results of the various *ab initio* investigations of FCO.

V. DISCUSSION

A. Interpretation of spectra and assignment of progressions I and II

The spectral simulations and the rotational constants for the excited electronic state derived from our rotationally resolved UV absorption spectra demonstrate that the FCO bands recorded over the wavelength range of 316–338 nm arise from a perpendicular transition between states of symmetry A' and A'', with the equilibrium geometry of the radical changing from bent in the ground electronic state (equilibrium bond angle=128°) to linear in the excited state. The resolved rotational structure thus allows us to reject all previous assignments of these bands to a $\tilde{B}\,^2A'-\tilde{X}\,^2A'$ transition. Instead, we propose that the UV bands arise from a transition from the ground $\tilde{X}\,^2A'$ state to the $^2A''$ component of the $\tilde{A}\,^2\Pi$ state which has a linear minimum energy geometry. This assignment is supported by the arguments of Nanbu *et al.*,[32] based solely on energetic considerations from *ab initio* calculations, that progressions I and II be attributed to absorption to the $\tilde{A}\,^2\Pi$ state.

The UV CRDS spectra show two progressions over the wavelength range from 316 to 338 nm. Features separated by $\sim$360 cm^{-1} divide into two types that alternate. Bands with a double-humped, diffuse structure underlying weak sharp structure (i.e., the 31 194, 30 472, and 29 679 cm^{-1} features) are found to be separated by $\sim$720 cm^{-1}, and stronger, sharp bands sitting atop diffuse features (but without a prominent underlying second diffuse hump, i.e., the 31 558, 30 833, and 30 104 cm^{-1} bands) are also separated by $\sim$720 cm^{-1}. The sharp features, whether weak or strong types, are best simu-

lated with $K'=0$. These observations suggest two progressions of $K'=0$ sub-bands, each with spacings of $\sim$720 cm^{-1}. For a bent-to-linear excitation, an extended progression in the bending vibration is anticipated. The electronically excited state is assigned as an A'' component of the $^2\Pi$ state ($\Lambda=1$), so even and odd quanta of the excited state bending vibration should, respectively, support odd and even K' levels because $K'=|\ell\pm\Lambda|$. The experimental pattern of rotational structure for each of the two band types thus matches the expectation of a bending progression, with only every alternate number of quanta of bending vibration supporting a $K'=0$ level, provided the bending vibrational frequency is $\sim$360 cm^{-1}. The most complete calculations for the bending vibration of the $\tilde{A}\,^2\Pi(A'')$ state report a frequency of 270 cm^{-1}.[30,31] Closer inspection of the pattern of levels computed at excitation energies above the $\tilde{A}\,^2\Pi(A'')$ minimum corresponding to photon absorption from the $\tilde{X}\,^2A'$ state at wavenumbers of 29 500–31 600 cm^{-1}, however, shows that the average interval between $K'=0$ levels is $\sim$790 cm^{-1}, corresponding to a bending vibrational frequency of $\sim$395 cm^{-1}. The calculated frequencies for the other vibrational modes of the $\tilde{A}$ state ($v_1'=2120\,cm^{-1}$, $v_2'=1045\,cm^{-1}$) suggest no other likely combinations of vibrations that can generate the observed pattern of vibrational features, and we thus assign the bands to bending progressions.

The magnitude of the rotational constant (B') in the upper electronic state is determined, in part, by the amplitude of the bending vibration in the excited state; in an analysis of LIF spectra assigned incorrectly to excitation to the $\tilde{A}\,^2\Pi(A'')$ state of FCO, Williams and Fleming[14] derived expressions for the effective rotational constant $\langle\overline{B'}\rangle$ averaged over one cycle of bending vibration

$$\langle\overline{B'}\rangle=0.4483-0.1519J_0(\alpha), \tag{6}$$

in units of cm^{-1}. Here, the numerical constants are obtained from predictions of the geometry of the $\tilde{A}$ state from *ab initio* calculations,[30] J_0 is the zeroth-order Bessel function and α is the turning point of the bending angle, specified as the angle of deviation from linearity. The value obtained for $\langle\overline{B'}\rangle$ when $\alpha=52°$ (corresponding to the geometry of the bent ground electronic state, projected onto the $\tilde{A}\,^2\Pi(A'')$ state following a vertical excitation) is 0.3261 cm^{-1}: This value is remarkably close to the value of B' derived from our spectra and listed in Table I for the strongly structured FCO bands [with origins at 31 558.44(5) cm^{-1}, 30 833.49(5) cm^{-1}, and 30 104.20(3) cm^{-1}].

The excited-state rotational constants, B', derived from analysis of the two types of rotationally resolved FCO bands show two clear trends: firstly, for each band type, B' values increase with increasing excitation energy, and secondly the B' values for the weakly structured bands are all smaller than those for the bands with pronounced sharp structure (see Table I). The general trend of increasing B' constants is consistent with the assignment of the bands to progressions in the bending vibration of the upper state. The smaller B' values for the weakly structured bands suggest that the bands are part of a bending progression built upon an excitation of a stretching vibration: The moment of inertia of the FCO about the *b* axis will increase upon stretching of the C═O or C–F bond, thus causing the value of B' to decrease. Moreover, such a combination vibration will involve fewer quanta of bending vibration than a pure bending vibrational level of the same energy and thus will show a lower B' value.

Ab initio calculations suggested only very small changes in the C═O and C–F bond lengths on excitation to the $\tilde{A}\,^2\Pi(A'')$ state,[30,31] so the combination band is likely to be either of the type $1_0^1 3_0^n$ or $2_0^1 3_0^n$, i.e., a bending progression built upon one quantum of C═O or C–F stretching vibration, respectively. Since both the weakly and strongly structured rotational bands can be simulated as $K'=0-K''=1$ transitions, *n* is required to be odd for both these types of vibrational features. Therefore, 3_0^n and $2_0^1 3_0^n$ or $1_0^1 3_0^n$ bands with identical *n* must be displaced by an odd multiple of the bending frequency in order that the sequences of sharp-diffuse-sharp bands for the two progressions lie exactly out of phase with one another. The *ab initio* calculations predict that $v_2'=1045\,cm^{-1}(\approx 3v_3')$ for the $\tilde{A}\,^2\Pi(A'')$ state, and the combination bands observed are thus plausibly $2_0^1 3_0^n$. The 3_0^{n+3} pure bending transition will thus lie at the same wavelength as the $2_0^1 3_0^n$ band, and only one of the two superimposed band types will give $K'=0$ rotational structure (depending upon whether *n* is odd or even). The $2_0^1 3_0^{n+1}$ and 3_0^{n+4} bands, which are also near-coincident, will be displaced by $\sim$360 cm^{-1} and will only exhibit $K'=0$ structure from the other band type.

The presence of the two vibronic transitions overlapping one another should lead to the presence of both odd and even K' levels (associated with $2_0^1 3_0^n$ and 3_0^{n+3} vibrations) within the same feature of the vibrational progression (Fig. 1). The two progressions are likely to be slightly displaced in energy from each other because of the difference in the $\tilde{A}\,^2\Pi(A'')$ vibrational spacing for levels consisting purely of the bending mode when compared to levels consisting of one quantum of stretch and several quanta of bending mode. For the strongly structured FCO bands, we would expect the presence close together of $K'=0,2,4,...$ sub-bands from the 3_0^n bands with odd values of *n*, but the slightly displaced $2_0^1 3_0^{n-3}$ band should also contribute $K'=1,3,5,...$ sub-bands to the same broad feature. For the double-humped bands with weak rotational structure the reverse is the case ($K'=0,2,...$ from $2_0^1 3_0^{n-3}$ and $K'=1,3,...$ from 3_0^n for *n* even). A tentative assignment of K' sub-bands observed as diffuse structure underlying and extending beyond the rotational fine structure is found in Figs. 2–4. Band assignments are based solely on the known FCO ground-state K'' structure, (for which the energy levels are given by $(A-\overline{B})K''^2$ with rotational constants taken from Nagia *et al.*[25]) and suggest features due to both odd and even K'' (and hence even and odd K') levels in each vibronic band. *Ab initio* calculations by Krossner *et al.*[30,31] predict the energies of origins of the K' sub-levels in the $\tilde{A}\,^2\Pi$ state for both the A' and A'' levels of FCO. The calculations suggest that the K' level energies are widely spaced and erratic. We do not see any firm evidence to support or contradict the assertion of widely spaced K' sub-

levels, but note that we can satisfactorily simulate the observed *K*-structure using Eq. (4) with *s* taking a small value.

The vibronic transitions $2_0^1 3_0^n$ and 3_0^{n+3} run through the spectral region labeled previously as progressions I and II. These two progressions, however, are coincident and the vibrational spacing is half that specified in previous assignments. The peaks labeled as Progression I correspond to $3_0^{n+3}+2_0^1 3_0^n$ (*n* even) vibronic transitions and the Progression II peaks are $3_0^{n+3}+2_0^1 3_0^n$ (*n* odd). Earlier interpretations of these bands have differed in the character of the vibrational modes excited, but attributed the absorption features to excitation to the $\tilde{B}\,^2A'$ state.[17,20,31] The identification of the $\tilde{B}\,^2A'$ state as the upper electronic state in the UV transitions was based on *ab initio* calculations by Carsky *et al.*[18] (which have since been superseded[30–32]) and matrix isolation spectra,[17] including isotope shifts observed for ^{18}O enriched FCO samples. Many of the spectroscopic data were reconciled with the results of the calculations of potentials and vibrational frequencies[30,31] but we suggest that a reassignment of the transition to the $\tilde{A}\,^2\Pi(A'')$, as proposed here, fits more closely with the *ab initio* data. The close correspondence of the predicted and experimental rotational constants, and the match between the experimental expectations and theoretical estimations of v_2' and v_3' have already been discussed. The calculations predict that the (nominally) C–F and C═O stretches of the $\tilde{A}\,^2\Pi(A'')$ state are strongly coupled, so both the v_1' and v_2' vibrational modes will exhibit isotope shifts for ^{18}O enriched samples. There is a calculated barrier on the $\tilde{A}\,^2\Pi(A'')$ state potential to loss of an F atom that lies $\sim$38 000 cm^{-1} above the minimum energy of the ground electronic state;[30,32] in both the matrix isolation and gas-phase UV absorption spectra of FCO, progressions I and II vanish beyond $\sim$35 000 cm^{-1}, which may either be a sign of the onset of a continuum in the C–F coordinate, or may correspond to much reduced Franck–Condon factors for higher energy excitations. In the current study, the equilibrium C–F and C═O bond lengths in the $\tilde{A}\,^2\Pi(A'')$ state are calculated to differ, respectively, by just -0.050 Å and $+0.037$ Å from those in the $\tilde{X}\,^2A'$ state, supporting the absence of extended progressions of the stretching vibrations in our assignment.

The computed energies of the $\tilde{A}\,^2\Pi(A'')$ state allow an estimate to be made of the number of bending vibrational quanta excited in the bands observed spectroscopically. The lowest energy transition observed in our experiments is at 29 972 cm^{-1}, and lies $\sim$4850 cm^{-1} above the calculated $\tilde{A}\,^2\Pi(A'')$ state minimum. Bearing in mind that the band is of the weakly structured type, this energy gap corresponds to $\sim$14 quanta of bend, although the intervals between bending vibrational levels, as computed by Krossner *et al.* are erratic, and a definitive assignment of the number of quanta is not yet possible.

There are a number of alternative assignments of the two vibrational progressions identified in the current study that should be considered carefully before accepting the one described in the preceding paragraphs. One possibility is that the weakly structured bands are instead hot bands terminating at bending levels of the excited state with $K'=0$, although their observation in matrix-isolation spectra argues against hot band contributions. The weak bands could thus be expressed as being either of type $1_1^0 3_0^n$ or $2_1^0 3_0^n$. To shift the bands out of phase with the 3_0^n progression, the ground-state vibrational frequency contributing to the hot band must be an odd multiple of the frequency of the excited state bending vibration, and the ground-state frequencies for the C═O stretch ($v_1''=1861\,\mathrm{cm}^{-1}$) and the C–F stretch ($v_2''=1026\,\mathrm{cm}^{-1}$) both approximately meet this criterion. The hot bands will, however, terminate at the same upper state levels as cold bands displaced to higher frequency (by either 1861 or 1026 cm^{-1}) and both band types should exhibit the same upper state rotational constants. A comparison of the values of B' obtained from fits to the weakly structured bands (performed with the rotational constants for the vibrationally excited levels of the ground electronic state) with those listed in Table I for the excited state, thus, allows us to discount this option. The alternative hypothesis that the strongly structured bands are hot bands associated with the weaker rotationally structured bands can be dismissed for the same reasons.

We must also consider the possibility of hot bands of the type $1_1^1 3_0^n$ or $2_1^1 3_0^n$, for which the change in the vibrational frequencies of the C–F or C═O stretches in the ground and excited states must be equal to (or an odd multiple of) v_3' to match the patterns seen in the spectra and to ensure $1_1^1 3_0^n$ (or $2_1^1 3_0^n$) bands coincide with 3_0^{n+1} or 3_0^{n-1} (or $3_0^{n\pm 3}$, etc.) bands, giving the correct odd–even K' behavior. This proposition was discounted on the basis that the expected changes in vibrational frequencies of v_1 and v_2 following excitation to the upper state do not match a progression with a spacing of $\sim$360 cm^{-1}.

The *ab initio* calculations of Krossner *et al.*[30,31] predict that the frequencies of the three vibrational modes of FCO $\tilde{A}\,^2\Pi(A'')$ satisfy the relationship $\nu_1' \approx 2\nu_2' \approx 6\nu_3'$, and thus polyad structure within the manifold of vibrational levels is anticipated. The CRD spectra of FCO show no clear evidence of such polyad structure, since there are no pronounced spectral features that cannot be assigned to *K* subband structure. The perturbation observed for the $N'=14$ level of the upper state reached by the transition with origin at $T_{0-1}=31\,558.44(5)$ cm^{-1} may, however, be an indication of a weak interaction between vibrational levels of the $\tilde{A}\,^2\Pi(A'')$ state. The perturbation is sharp, having a marked effect on just one spectroscopically bright level, and results in a small energy shift rather than line-broadening. It is thus likely to involve an interaction between two $K'=0$ levels, since $K'\neq 0$ levels are broadened by predissociation. The lowest 3_0^n band recorded in the current study is tentatively assigned to $n=14$, which means that the localized perturbation occurs for the $K'=0$, $N'=14$ rotational level of the $v_3'=19$ vibrational state. The appearance of this perturbation may be linked to a rapid increase in the vibrational density of states (and hence the number of dark states) at this energy.[48] The 6:3:1 ratio of frequencies of the three vibrational modes in the $\tilde{A}\,^2\Pi(A'')$ state results in a series of sharp steps in the density of states with increasing energy (assuming that the

differences in anharmonicities for the modes are small). In terms of the polyad number $P=6v_1'+3v_2'+v_3'$, polyads with $P=15-17$ are composed of twelve possible combinations of various quanta of the three vibrational modes. For $P=18$, the number of combinations of vibrational modes rises to sixteen. The perturbing dark state must, however, support $K'=0$ levels (see above) and a count of levels that contain odd numbers of quanta of the bending vibration contributing to each polyad shows that while just six bands have $v_3'=$ odd for $P=18$, there is an abrupt jump to ten such levels for $P=19$. This pronounced increase in the density of dark state with $K'=0$ at an energy close to that of $v_3'=19$ may thus support the 3_0^{19} assignment of the locally perturbed vibronic band with origin at 31 558.44 cm^{-1}.

B. Assignments of progressions III and IV

Having reassigned progressions I and II (originally assigned to excitation to the $\tilde{B}\,^2A'$ state), we must consider the consequences for the assignments of the remaining two progressions, III and IV (reported previously but not investigated experimentally in the current study) which were previously attributed to excitation to the $\tilde{C}\,^2A''$ state and a higher lying $^2A'$ state, respectively. Progression III, which extends to energies greater than 42 000 cm^{-1}, is unlikely to be a result of excitation to the $\tilde{B}\,^2A'$ state because all the calculations performed at the CI level indicate that this state is repulsive in the C–F coordinate for energies $\geqslant$31 500 cm^{-1} above the ground-state minimum. Krossner *et al.*[31] and Nanbu *et al.*[32] concur that progression III is instead associated with the secondary minimum on the $\tilde{A}\,^2A''$ adiabatic surface evident at bending angles less than 115° (see Fig. 7). The former authors treated progression III as arising from excitation to levels of the diabatic $2\,^2A''$ state that rises in energy from a minimum at 105° as the bending angle increases. The avoided crossing of this potential with the diabatic $1\,^2A''$ state with minimum energy at linear geometry occurs at angles close to 115° and forms the adiabatic potentials shown for example, in Fig. 7, where the avoided crossing is apparent, and labeled as the $\tilde{A}\,^2A''$ and $\tilde{C}\,^2A''$ states. Predicted bending frequencies were in good agreement with the observed intervals in the spectrum, and an extended progression is consistent with the large change in the bond angle between the ground and excited states. Nanbu *et al.* computed that the first adiabatic $^2A''$ surface has saddle points to dissociation along the C–F coordinate at $\Theta\approx100°$ and 180° and respective energies of ~40 500 and 42 300 cm^{-1}. The extension of progression III to above 42 000 cm^{-1} may indicate either that the *ab initio* calculations have not faithfully reproduced the true saddle point energies, or that the bending vibrational levels of the diabatic $2\,^2A''$ state are only weakly coupled (either electronically or by vibrational interaction) to the C–F continuum.

The assignment of progression IV, which starts at ~40 500 cm^{-1}, remains uncertain, but may correspond to excitation of another vibration or combination band of the $\tilde{C}\,^2A''$ state, or to transitions to the next $^2A'$ state, denoted in Fig. 6 as $\tilde{D}\,^2A'$. The latter hypothesis can be tested by computing the minimum energy and equilibrium geometry of the $\tilde{D}\,^2A'$ state. A geometry optimization routine within the MOLPRO 98.1 package[49] operating on the SA-CASSCF wavefunction was used, and the results were then employed in an MRCI calculation to determine the relative energy with respect to the ground state. The derived geometrical parameters are $R_{C-O}=1.1898$ Å, $R_{C-F}=1.8724$ Å, $\Theta=106.518°$, and a minimum energy of 39 823 cm^{-1}. For comparison, the minimum energy of the adiabatic $\tilde{C}\,^2A''$ state is computed to be 36 216 cm^{-1} at $R_{C-O}=1.3287$ Å, $R_{C-F}=1.3224$ Å, $\Theta=121.019°$. The true minima of these states at the MRCI level may lie at slightly different geometries since the MRCI wavefunctions were not used in the geometry optimization. However, the calculated $\tilde{D}\,^2A'$ state minimum is at very extended C–F bond length, suggesting that it is unlikely to be a viable candidate for progression IV.

C. Predissociation of FCO and comparisons with HCO

There are many similarities between the spectroscopy of HCO and FCO: the lower energy ranges of the electronic spectra of these radicals are dominated by extended progressions in a bending vibrational mode that is excited by the bent to linear geometry change of the $\tilde{A}\,^2A''-\tilde{X}\,^2A'$ transition. For HCO, this transition is assigned to occur between two Renner–Teller components of a $^2\Pi$ state, and, just as is seen for FCO, the resultant bands show alternating sharp and diffuse rotational structure for $K'=0$ (odd quanta of bend) and $K'\neq0$ (even quanta of bending vibration), respectively.[50,51] Rotation about the *a* axis of HCO couples $K'\neq0$ levels of the $\tilde{A}\,^2\Pi(A'')$ state with levels of the ground state that lie above the dissociation limit for formation of $H(^2S)+CO(X\,^1\Sigma^+)$. Sub-bands with $K'\neq0$ are thus rapidly predissociated and hence are diffuse. Levels of the $\tilde{A}\,^2\Pi(A'')$ state with $K'=0$ cannot couple to the ground state via this mechanism and show sharp rotational structure. These levels are, however, known to predissociate via weaker spin–orbit coupling and via one or more alternate mechanisms involving couplings that become stronger as N' increases.[52,53] Thus rotational lines in the spectrum of HCO with $K'=0$ become increasingly broad as N' increases, and the N'-dependent predissociation has been attributed either to a Coriolis interaction with $N'(N'+1)$ dependence, or to a *K*-type resonance mechanism with $N'^2(N'+1)^2$ dependence.

Similar alternations between band types exhibiting sharp $(K'=0)$ and diffuse $(K'>0)$ structure are exhibited in the UV absorption spectrum of FCO, and suggest a similar electronic character for the responsible spectroscopic transition. The *ab initio* explorations of the low-lying states of FCO, however, reveal a more complicated picture than for HCO because in the former radical at linear geometry, the $^2\Sigma^+$ state lies lower in energy than the $^2\Pi$ state for C–F and C–O bond lengths close to their equilibrium values. As the molecule bends, the $^2\Sigma^+$ state might be expected to evolve into the $^2A'$ ground state, implying that excitation to the $\tilde{A}\,^2\Pi(A'')$ state is not a transition between two components of a Renner–Teller pair. The use of *ab initio* and spectro-

scopic data to clarify this point and to highlight the similarities between FCO and HCO is discussed in more detail in Sec. V D.

Linewidths for FCO all show evidence of lifetime broadening, and for the diffuse bands ($K' \neq 0$), we estimate that Γ exceeds 2.0 cm^{-1}. Even the levels with $K'=0$ show lifetimes as short as 10.6 ps, and this strong predissociation of the $\tilde{A}\,^2\Pi(A'')$ state probably explains why no LIF spectrum of FCO has been reported. We also see evidence of increased broadening of rotational lines in the $K'=0$ sub-bands of FCO at higher N', but the changes are not as marked as for HCO, and the possible broadening effects of unresolved spin–rotation splitting cannot be completely discounted. The fact that the lines are broadened at low values of N' (for $K'=0$) suggests the additional role of spin–orbit coupling[54] to the high-lying levels of the ground state of FCO, as is suggested for HCO.[52]

D. Electronic structure of the FCO ground state

As mentioned in the preceding section, there is some remaining uncertainty about the electronic structure of the ground state and the precise nature of the electronic transition to the $\tilde{A}\,^2\Pi(A'')$ state that we observe experimentally. If, as predicted by Francisco *et al.*,[28] the ground state derives from the A' component of a $^2\Pi$ state, then the $\tilde{A}$–$\tilde{X}$ transition is between the two components of a Renner–Teller pair, just as is observed for HCO. If, however, the $^2\Sigma^+$ state lies lower in energy than the $^2\Pi$ state for linear FCO, then the $\tilde{X}\,^2A'$ state might be expected to derive from the $^2\Sigma^+$ state upon bending.[30–32]

The $\tilde{X}\,^2A'$ state of FCO correlates diabatically to $F(^2P)+CO(a\,^3\Pi)$ fragments as the C–F bond is stretched. The ground electronic configuration is $(\text{core})^{12}(7a')^2(8a')^2(1a'')^2(9a')^2(2a'')^2(10a')^1(3a'')^0$ with the constituent molecular orbitals illustrated schematically in Fig. 9. The sketches of the orbitals are based on an examination of the results of restricted Hartree–Fock (RHF) and CASSCF calculations for molecular geometries close to that of the minimum of the $\tilde{A}\,^2\Pi$ state. The results from MOLPRO calculations were displayed using the graphical package MOLDEN,[55] and these plots form the basis for the orbital sketches in the center of Fig. 9.

The electronic character of the ground state is determined by the nature of the highest, singly occupied ($10a'$) MO. This SOMO may, in principle, be composed primarily of either an antibonding $a'(\pi^*)$ or an $a'(\sigma^*)$ orbital. These two cases would correspond respectively to a ground-state wave function of $^2\Pi$ or $^2\Sigma^+$ type character in a linear geometry. For a coordinate system in which the (bent) molecule lies in the xy plane, with the x axis taken as the direction of the bond axis in the linear molecule, the $10a'$ orbital is found to be predominantly composed of $2p_y$ atomic orbitals on the three atoms at the configuration of the $\tilde{X}$ state minimum with some $2p_x$ character mixed in on the F atom. In other words, there is evidence of hybridisation of the $a'(\pi^*)$ and $a'(\sigma)$ orbitals upon bending. Figure 10 presents a contour plot of the $10a'$ orbital, computed at the MRCI level at the geometry of the $\tilde{X}$ state minimum. The $a'(\pi^*)$ character of the $10a'$ orbital is evident, and the major constituent of the $10a'$ SOMO is apparently derived from the $a'(\pi^*)$ MO rather than being an antibonding σ^* orbital.[32] The significant π-character is consistent with the outcome of SA-CASSCF calculations at the

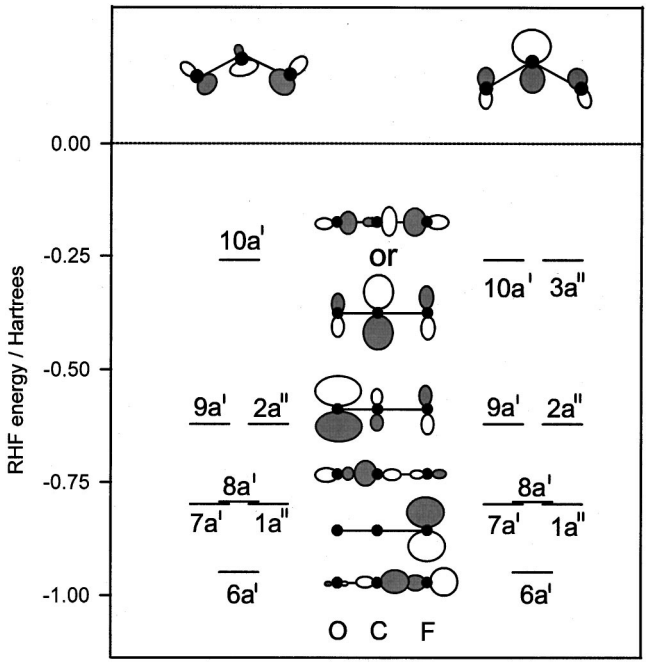

FIG. 9. Two alternative molecular orbital diagrams for the ground-state FCO radical. Left: the $10a'$ orbital is shown as a σ orbital that is bonding between O and C but antibonding between C and F. Right: the $10a'$ orbital is a molecular π^* antibonding orbital (and hence degenerate with $3a''$ at linear geometry). Schematic diagrams of the molecular orbitals in the linear geometry are shown at the center of the figure. The sketches are derived from wavefunction plots of the RHF orbitals obtained using MOLDEN (see text). The atomic centres are illustrated as black dots. At the top of the diagram are similar schematics for the two candidate $10a'$ orbitals at a bent geometry. The $a'(\pi^*)$ MO should be stabilized on bending, whereas the $a'(\sigma)$ MO loses C–O bonding overlap upon bending.

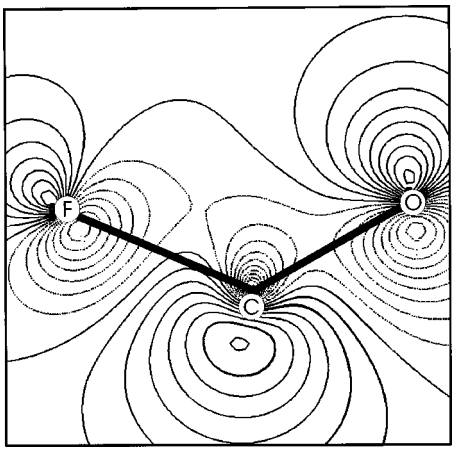

FIG. 10. Contour plot of the wave function of the SOMO in the ground electronic state of FCO, calculated at the geometry of the $\tilde{X}\,^2A'$ state minimum at the MRCI level (aug-cc-pVTZ basis set). The average occupancy number is 1.04. The plot was produced with the MOLDEN display package (Ref. 55).

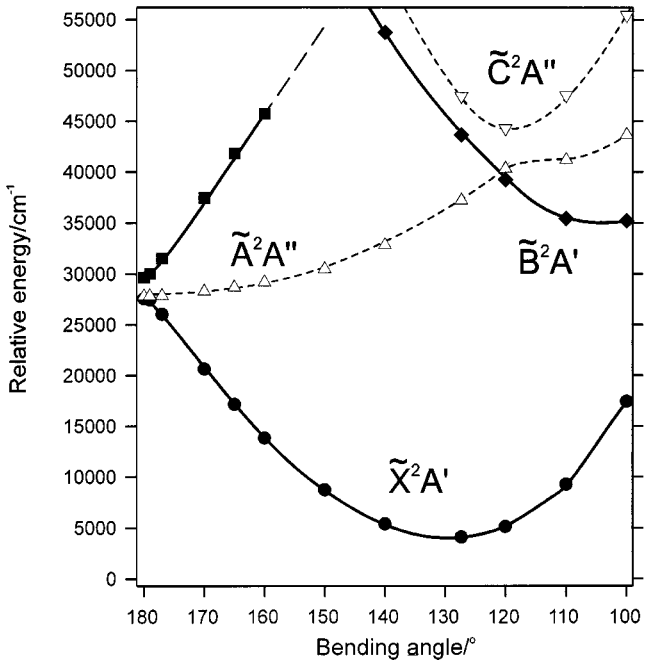

FIG. 11. MRCI calculations for the bending potentials of the FCO radical calculated with the C–F and C–O bond lengths fixed at 1.284 and 1.206 Å, respectively. Two $^2A'$ (black symbols) and two $^2A''$ states (open symbols) were included at the SA-CASSCF level. Solid curves are $^2A'$ states: dashed curves are $^2A''$ states. The $10a'$ orbital (SOMO for the $\tilde{X}\,^2A'$ state at these bond lengths) is clearly stabilized on bending, as expected for the a' component of the π^* antibonding orbital shown in Fig. 9.

geometry of the $\tilde{A}\,^2\Pi(A'')$ state minimum, at which point the $\cdots(2a'')^2(9a')^2(3a'')^1\,^2A''$ and $\cdots(2a'')^2(9a')^2(10a')^1\,^2A'$ states have almost precisely the same energy, implying that the $10a'$ and $3a''$ orbitals are components of the same π orbital. Examination of the $11a'$ orbital suggests that it is also hybridised for bent FCO; at linear geometry, the $11a'$ orbital has predominantly σ character which is maintained as the radical bends, but orbital repulsion along the C–F bond rotates the atomic orbital on the central C atom, resulting in significant p_y character.

To examine further the orbital symmetry character of the ground state, bending potentials were calculated for the lowest valence states at fixed bond lengths of $R_{\mathrm{C-F}}=1.19$ Å and $R_{\mathrm{C-O}}=1.205$ Å. At linear geometry, these bond lengths lie within the small region of configuration space for which the $^2\Pi$ state is computed to be lower in energy than the $^2\Sigma^+$ state. The results of the calculation are shown in Fig. 11, and the bending potentials reveal that for these bond lengths, the lowest $^2A''$ and $^2A'$ states correlate to the same energy at a linear geometry. The expectation of the MO pictures in Fig. 9 is that the $10a'$ orbital would stabilize upon bending, and the calculations demonstrate such a reduction in energy as the first $^2A'$ state bends. The second $^2A'$ state, however, rapidly destabilizes, as expected for a nonbonding σ orbital. The results suggest that for those values of $R_{\mathrm{C-F}}$ and $R_{\mathrm{C-O}}$ for which, in a linear configuration, the $^2\Sigma^+$ state lies below the $^2\Pi$ state, any bending of the molecule causes the rapidly destabilized $a'(\sigma)$ orbital to form an avoided crossing with the $a'(\pi^*)$ orbital. The energy well in the $\tilde{X}\,^2A'$ state is largely the result of the stabilization of the $a'(\pi^*)$ orbital, which, save for very close to linear, is lower in energy than the $a'(\sigma)$ orbital. As a consequence, the bent ground state has a significant $a'(\pi^*)$ component, and much of the character of the $\tilde{A}\,^2\Pi(A'')-\tilde{X}\,^2A'$ excitation is that of a transition between two constituents of a Renner–Teller pair.

The arguments presented above, and based upon our electronic structure calculations, are strongly supported by the evidence from the UV CRD spectra of FCO, and in particular the different predissociation rates for $K'=0$ and $K'>0$ sub-levels. All the levels of the $\tilde{A}\,^2\Pi(A'')$ state probed in this study lie above the asymptote for C–F bond rupture on the ground-state PES. For HCO, the $K'>0$ levels can be written as a mixture of wavefunctions associated with the $\tilde{X}\,^2A'$ and $\tilde{A}\,^2\Pi(A'')$ electronic states,[56] and as a consequence, flux excited to $K'>0$ levels of the $\tilde{A}\,^2\Pi(A'')$ state is rapidly coupled to the ground state and has sufficient energy to dissociate. Conversely, $K'=0$ levels cannot be described as such a mixture of wavefunctions, and are not coupled to the $\tilde{X}\,^2A'$ state PES via the Renner–Teller interaction. Analogous behavior for FCO indicates the presence of a Renner–Teller mediated predissociation of the $\tilde{A}\,^2\Pi(A'')$ state via the ground electronic state. Alternative coupling schemes, such as *b* axis rotation, might be expected to show less pronounced differences between predissociation rates of $K'=0$ and $K'>0$ sub-levels. The evidence from the spectroscopy thus points towards a Renner–Teller interaction between the $\tilde{X}\,^2A'$ and $\tilde{A}\,^2\Pi(A'')$ states, and hence to marked $a'(\pi^*)$ character in the ground electronic state.

The spin–rotational interactions in the ground electronic state of FCO have been characterized by Nagai *et al.*[25] The experimental observation that $\varepsilon_{aa}\gg\varepsilon_{bb}+\varepsilon_{cc}$ is consistent with the dominant interaction leading to spin–rotation splitting being between two components of a Renner–Teller pair.[57,58] For interaction with a single excited state, and in the model of ''pure precession,'' we can approximate[58]

$$\varepsilon_{aa}\approx\frac{4A_{\mathrm{SO}}A}{E_u-E_1}, \tag{7}$$

where E_u-E_1 is the separation between the minima of the A'' and A' components of the Renner–Teller pair, A_{SO} is the spin–orbit coupling constant, and A is the rotational constant about the *a* axis. This relationship enables a check as to whether the measured value of ε_{aa} tallies with the pure-precession model, with use of $A=6.377\,746\,\mathrm{cm}^{-1}$ (Ref. 25), and *ab initio* computation of A_{SO} and the energy separation. The value of $E_u-E_1=25\,115\,\mathrm{cm}^{-1}$ was obtained from the MOLPRO calculations described in Sec. IV, and these calculations were extended to obtain a magnitude for the spin–orbit interaction. Using MRCI wave functions and the aug-cc-pVTZ basis set, the spin–orbit constant was computed to be $A_{\mathrm{SO}}=56.09\,\mathrm{cm}^{-1}$ at the minimum of the A'' state. Insertion of numerical values of the three parameters into Eq. (7) gives $\varepsilon_{aa}=0.0570\,\mathrm{cm}^{-1}$, in excellent agreement with the experimental result of $0.0610\pm0.0007\,\mathrm{cm}^{-1}$. This close correspondence between experimental and theoretical values (within the pure-precession approximation) supports the assertion that the $\tilde{A}\,^2A''$ and $\tilde{X}\,^2A'$ states derive from the same $^2\Pi$ state for linear FCO.

Comparison between FCO and the isoelectronic NO_2 yields striking similarities in electronic structure. Despite the different molecular symmetry, the lower valence electronic states of NO_2 and FCO are equivalent (compare Fig. 3 of Ref. 59 and Fig. 7 of the current study): The $\tilde{X}\,^2A_1$ and $\tilde{B}\,^2B_1$ states of NO_2 are also components of a $^2\Pi$ electronic state in linear geometry, while the $\tilde{A}\,^2B_2$ state is analogous to the $\tilde{B}\,^2A'$ state of FCO. Experimental measurements[60] of the A rotational constant and the spin–rotation constants in the ground state of NO_2, combined with theoretical calculations of $E_u - E_1$,[59,61] yield a pure-precession value of $A_{SO} = 76.4 \pm 0.9\,cm^{-1}$, very similar to that computed for FCO. The greater stabilization of the $\tilde{A}\,^2B_2$ state in NO_2 compared with the $\tilde{B}\,^2A'$ state of FCO, however, ensures that it is a transition to the $\tilde{A}\,^2B_2$ state that forms the first electronic absorption band in NO_2, rather than a transition to the upper Renner–Teller $\tilde{B}\,^2B_1$ component.

VI. CONCLUSIONS

CRDS has been used to record rotationally resolved spectra of six bands of FCO over the wavelength range from 316 to 338 nm. Rotational constants for the excited electronic state have been derived from the spectra, and spectral simulations demonstrate that the excitation corresponds to a *c*-type transition from the ground $\tilde{X}\,^2A'$ state to a state of A'' symmetry. The equilibrium geometry changes from bent in the ground state (with valence angle of 128°) to linear in the excited state. We thus reject previous assignments of these bands to the $\tilde{B}\,^2A' - \tilde{X}\,^2A'$ transition,[17,20] and instead assign the spectral features to an excitation from the $\tilde{X}\,^2A'$ state to the $^2A''$ component of a Renner–Teller pair arising from the $\tilde{A}\,^2\Pi$ state. The minimum of the $\tilde{A}\,^2\Pi(A'')$ component occurs at linear geometry.

The spectra exhibit two vibrational progressions whose rotationally resolved features, which alternate between being weakly and strongly structured, are assigned to transitions to levels with $K' = 0$. Each band shows an underlying and extensive diffuse background. The weakly structured bands [with origins at 31 193.80(4) cm^{-1}, 30 472.07(7) cm^{-1}, and 29 679.88(6) cm^{-1}] sit on top of diffuse, double-humped backgrounds and are assigned to combination bands which consist of one quantum of v_2' (approximately described as the C–F stretch) and several quanta of the bending vibration, v_3', and are of the type $2_0^1 3_0^n$ with n odd (in order that the vibronic levels support states with $K' = 0$). The more strongly structured bands, with origins at 31 558.44(5) cm^{-1}, 30 833.49(5) cm^{-1} and 30 104.20(3) cm^{-1}, sit on top of diffuse features without a prominent second hump. These bands are assigned to a pure bending progression of type 3_0^n with n, again, odd. In both band types, the diffuse features arise from strong predissociation of sub-levels of the excited state with $K' > 0$, and the pattern of broad features evident in the spectra is consistent with the known K'' level structure of the ground electronic state. The two vibrational progressions overlap, with the 3_0^{n+3} transition almost coincident with the $2_0^1 3_0^n$ transition.

The above assignments concur with *ab initio* calculations[30,31] of the energies of excited electronic states and frequencies of the vibrational modes of the $\tilde{A}\,^2\Pi(A'')$ state. Values of B' for the $\tilde{A}\,^2\Pi(A'')$ state determined from the spectral analysis agree very closely with estimates from the *ab initio* calculations of rotational constants averaged over the large amplitude bending of the levels excited in the $\tilde{A}\,^2\Pi(A'')$ state by a vertical transition. The features in the FCO UV spectrum previously assigned to excitation to the $\tilde{B}\,^2A'$ state and labeled as progressions I and II are thus reassigned, respectively, as $\tilde{A}\,^2\Pi(A'') - \tilde{X}\,^2A'$, $3_0^{n+3} + 2_0^1 3_0^n$ (n even) and $\tilde{A}\,^2\Pi(A'') - \tilde{X}\,^2A'$, $3_0^{n+3} + 2_0^1 3_0^n$ (n odd). The $\tilde{B}\,^2A'$ state is judged not to contribute sharp structure to any part of the observed FCO absorption spectrum.

The $K' > 0$ levels of the $\tilde{A}\,^2\Pi(A'')$ state are rapidly predissociated by rotational coupling to the ground state. We also observe evidence for a broadening of all lines of the $K' = 0$ sub-levels, with linewidths increasing to higher N'. These observations are attributed to a spin–orbit coupling induced predissociation of all levels, and, in addition, a further rotation induced coupling to the continuum of the ground state that strengthens at high N'. The rapid predissociation of all rotational levels of the $\tilde{A}\,^2\Pi(A'')$ state explains why FCO does not exhibit an LIF spectrum. The spectroscopy and predissociation of FCO show many parallels with the much studied HCO system: spectral data and *ab initio* calculations suggest that the $^2A'$ ground state of FCO has a significant component of $a'(\pi^*)$ singly occupied electronic orbital character despite a $^2\Sigma^+$ state [with $a'(\sigma)$ character] lying lower in energy at the linear geometry. The FCO $\tilde{A}\,^2\Pi(A'') - \tilde{X}\,^2A'$ absorption spectrum thus exhibits many characteristics of a transition between two states coupled by a Renner–Teller interaction.

The high resolution afforded by CRDS has enabled us to disentangle the complicated near UV spectroscopy of the FCO radical and has demonstrated that previous assignments of the absorption spectrum, based on low-resolution measurements, were incorrect. To date, no LIF spectrum of FCO has been reported, but CRDS offers a high-sensitivity technique for detection of FCO that will have numerous applications in, for example, measurements of the kinetics of reactions of this radical.[62]

ACKNOWLEDGMENTS

W.H.H. thanks the EPSRC for the award of a studentship and I.C.L. thanks the Leverhulme Trust for a postdoctoral fellowship. We are very grateful to Professor R. N. Dixon, Professor M. N. R. Ashfold, and Dr. C. M. Western for numerous helpful discussions, to Mr. K. N. Rosser for technical support, and to Professor G. G. Balint-Kurti for access to the Beowulf system. We thank Professor M. Peric for communicating the results of unpublished calculations. Financial support for this work was provided by the Royal Society.

[1] E. O. Edney and D. J. Driscoll, Int. J. Chem. Kinet. **24**, 1067 (1992).
[2] E. C. Tuazon and R. Atkinson, J. Atmos. Chem. **16**, 179 (1993).

[3] J. Sehested and T. J. Wallington, Environ. Sci. Technol. **27**, 146 (1993).
[4] J. S. Francisco, A. N. Goldstein, and I. H. Williams, J. Chem. Phys. **89**, 5 (1988).
[5] M. M. Maricq, J. J. Szente, G. A. Khitrov, and J. S. Francisco, Chem. Phys. Lett. **199**, 71 (1992).
[6] C. J. Cobos, A. E. Croce, and E. Castellano, Chem. Phys. Lett. **239**, 320 (1995).
[7] M. P. Badenes, E. Castellano, C. J. Cobos, A. E. Croce, and M. E. Tucceri, Chem. Phys. Lett. **303**, 482 (1999).
[8] G. Bednarek, G. A. Argüello, and R. Zellner, Ber. Bunsenges. Phys. Chem. **100**, 445 (1996).
[9] T. J. Wallington, T. Ellermann, O. J. Nielsen, and J. Sehested, J. Phys. Chem. **98**, 2346 (1994).
[10] R. J. H. Clark and J. R. Dann, J. Phys. Chem. **100**, 9271 (1996).
[11] P. R. Westmoreland, D. R. F. Burgess, W. Tsang, and M. R. Zachariah, *Twenty-fifth symposium (International) on Combustion* (The Combustion Institute, Pittsburgh, 1994), p. 1505.
[12] O. Sanogo, J. L. Delfau, R. Akrich, and C. Vovelle, *Twenty-fifth symposium (International) on Combustion* (The Combustion Institute, Pittsburgh 1994), p. 1489.
[13] G. Hancock and D. E. Heard, J. Photochem. Photobiol. A **60**, 265 (1991).
[14] B. A. Williams and J. W. Fleming, J. Chem. Phys. **106**, 4376 (1997).
[15] D. E. Milligan, M. E. Jacox, A. M. Bass, J. J. Comeford, and D. E. Mann, J. Chem. Phys. **42**, 3187 (1965).
[16] D. K. W. Wang and W. E. Jones, J. Photochem. **1**, 147 (1972/73).
[17] M. E. Jacox, J. Mol. Spectrosc. **80**, 257 (1980).
[18] P. Carsky, M. Machacek, and R. Zahradnik, Collect. Czech. Chem. Commun. **38**, 3067 (1973).
[19] S. Toby and F. S. Toby, J. Phys. Chem. **85**, 4071 (1981).
[20] M. M. Maricq, J. J. Szente, Y. Su, and J. S. Francisco, J. Chem. Phys. **100**, 8673 (1994).
[21] S. Inomata, M. Furubayashi, T. Imamura, N. Washida, and M. Yamaguchi, J. Chem. Phys. **111**, 6356 (1999).
[22] S. A. Wright and P. J. Dagdigan, J. Chem. Phys. **107**, 9755 (1997).
[23] N. Washida, M. Furubayashi, T. Imamura, I. Bridier, and A. Miyoshi, J. Chem. Phys. **107**, 6998 (1997).
[24] M. Furubayashi, I. Bridier, S. Inomata, N. Washida, and K. Yamashita, J. Chem. Phys. **106**, 6302 (1997).
[25] K. Nagai, C. Yamada, Y. Endo, and E. Hirota, J. Mol. Spectrosc. **90**, 249 (1980).
[26] A. O'Keefe and D. A. G. Deacon, Rev. Sci. Instrum. **59**, 2544 (1988).
[27] M. D. Wheeler, S. M. Newman, A. J. Orr-Ewing, and M. N. R. Ashfold, J. Chem. Soc., Faraday Trans. **94**, 337 (1998).
[28] J. S. Francisco, A. N. Goldstein, M. A. Robb, and I. H. Williams, Chem. Phys. Lett. **191**, 13 (1992).
[29] D. A. Ramsay, J. Chem. Phys. **21**, 960 (1953).
[30] Th. Krossner, L. Zülicke, R. Vetter, M. Peric, and S. D. Peyerimhoff, J. Chem. Phys. **101**, 3973 (1994).
[31] Th. Krossner, M. Peric, L. Zülicke, and R. Vetter, J. Chem. Phys. **101**, 3981 (1994).
[32] S. Nanbu, M. Gomyo, and S. Iwata, Chem. Phys. **184**, 97 (1994).
[33] J. Pearson, A. J. Orr-Ewing, M. N. R. Ashfold, and R. N. Dixon, J. Chem. Phys. **106**, 5850 (1997).
[34] M. D. Wheeler, A. J. Orr-Ewing, and M. N. R. Ashfold, J. Chem. Phys. **107**, 7591 (1997).
[35] J. A. Pople and H. C. Longuet-Higgins, Mol. Phys. **1**, 372 (1958).
[36] T. H. Dunning, J. Chem. Phys. **53**, 2823 (1970).
[37] R. A. Kendall, T. H. Dunning, Jr., and R. J. Harrison, J. Chem. Phys. **96**, 6796 (1992); D. E. Woon and T. H. Dunning, Jr., *ibid.* **100**, 2975 (1994).
[38] MOLPRO 98.1 is a package of *ab initio* programs written by H. J. Werner and P. J. Knowles, with contributions of J. Almløf, R. D. Amos, A. Berning *et al.*
[39] I. C. Lane and A. J. Orr-Ewing, Mol. Phys. **98**, 793 (2000).
[40] H. J. Werner and P. J. Knowles, J. Chem. Phys. **89**, 5803 (1998); P. J. Knowles and H. J. Werner, Chem. Phys. Lett. **145**, 514 (1988).
[41] S. R. Langhoff and E. R. Davidson, Int. J. Quantum Chem. **8**, 61 (1974).
[42] H.-J. Werner, C. Bauer, P. Rosmus, H-M. Keller, M. Stumpf, and R. Schinke, J. Chem. Phys. **102**, 3593 (1995).
[43] K. P. Huber and G. Herzberg, *Constants of Diatomic Molecules* (van Nostrand Reinhold, New York, 1979).
[44] M. A. C. MacNell and J. C. J. Thynne, Int. J. Mass Spectrom. Ion Phys. **3**, 35 (1969).
[45] M. T. Bowers and M. Chau, J. Phys. Chem. **80**, 1739 (1976).
[46] T. J. Buckley, R. D. Johnson, II, R. E. Huie, Z. Zhang, S. C. Kuo, and R. B. Klemm, J. Phys. Chem. **99**, 4879 (1995).
[47] D. A. Dixon and D. Feller, J. Phys. Chem. A **102**, 8209 (1998).
[48] H. Ishikawa, R. W. Field, S. C. Farantos, M. Joyeux, J. Koput, C. Beck, and R. Schinke, Annu. Rev. Phys. Chem. **50**, 443 (1999).
[49] F. Eckert, P. Pulay, and H.-J. Werner, J. Comput. Chem. **18**, 1473 (1997).
[50] J. W. C. Johns, S. H. Priddle, and D. A. Ramsay, Faraday Discuss. Chem. Soc. **35**, 90 (1963).
[51] J.-C. Loison, S. H. Kable, P. L. Houston, and I. Burak, J. Chem. Phys. **94**, 1796 (1991).
[52] R. Vasudev and R. N. Zare, J. Chem. Phys. **76**, 5267 (1982).
[53] G. Rumbles, J. J. Valentini, B. M. Stone, and E. K. C. Lee, J. Phys. Chem. **93**, 1303 (1989).
[54] T. Barrow, R. N. Dixon, and G. Duxbury, Mol. Phys. **27**, 1217 (1974).
[55] G. Schaftenaar and J. H. Noordik, J. Comput.-Aided Mol. Design **14**, 123 (2000).
[56] S. H. Kable, J. C. Loison, D. W. Neyer, P. L. Houston, I. Burak, and R. N. Dixon, J. Phys. Chem. **95**, 8013 (1991).
[57] E. Hirota, *High resolution spectroscopy of transient molecules* (Springer-Verlag, Berlin, 1985).
[58] E. Hirota, J. Phys. Chem. **87**, 3375 (1983).
[59] G. D. Gillespie, A. U. Khan, A. C. Wahl, R. P. Hosteny, and M. Krauss, J. Chem. Phys. **63**, 3425 (1975).
[60] W. C. Bowman and F. C. De Lucia, J. Chem. Phys. **77**, 92 (1982).
[61] Y. Xie, R. D. Davy, B. F. Brien, C. P. Blahous, III, Y. Yamaguchi, and H. F. Schaefer, III, Chem. Phys. **135**, 179 (1989).
[62] Y. Ninomiya, M. Goto, S. Hashimoto, M. Kawasaki, and T. J. Wallington, Int. J. Chem. Kinet. (to be published).